Article

Impact of Microstructure of Nanoscale Magnetron Sputtered Ru/Al Multilayers on Thermally Induced Phase Formation

Vincent Ott [1,*], Christian Schäfer [2], Sebastian Suarez [2], Karsten Woll [3], Frank Mücklich [2], Hans J. Seifert [1], Sven Ulrich [1], Christoph Pauly [2] and Michael Stueber [1,*]

[1] Karlsruhe Institute of Technology (KIT), Institute for Applied Materials (IAM), Applied Material Physics (AWP), 76131 Karlsruhe, Germany
[2] Functional Materials Department, Saarland University, Campus D3.3, 66123 Saarbrücken, Germany
[3] Karlsruhe Institute of Technology (KIT), Institute for Applied Materials (IAM), Mechanics of Materials and Interfaces (MMI), 76131 Karlsruhe, Germany
* Correspondence: vincent.ott@kit.edu (V.O.); michael.stueber@kit.edu (M.S.)

Abstract: In this study, we report on phase formation and microstructure evolution in multiscale magnetron sputtered Ru/Al multilayers upon thermal annealing in vacuum at slow heating rates of 10 K/min. By specifically adjusting the microstructure and design of the as-deposited multilayers, the formation of certain desired phases can be tuned. We demonstrate that the synthesis of single phase RuAl thin films is possible in a very controlled manner in a solid state only via thermal activation without initiating the self-propagating exothermic reactions of Ru/Al multilayers. To investigate phase formation sequences and the resulting microstructures, Ru/Al multilayers were designed via magnetron sputtering with systematic variation of bilayer modulation periods and subsequent vacuum annealing. Thin films samples were characterized by in situ high-temperature XRD, TEM imaging and diffraction. It is shown that different phase sequences appear in strong correlation with the modulation length. Depending on the multilayer design, the phase formation toward single-phase RuAl thin films happens as either a multi-step or single-step event. In particular, below a critical threshold of the modulation period, the multi-step phase formation can be suppressed, and only the desired RuAl target phase is obtained with a pronounced growth in a preferred orientation. This finding may be versatile for the targeted synthesis of intermetallic phases, contributing to further understanding of phase formation in such nanoscale multilayer systems.

Keywords: magnetron sputtering; multilayer; phase formation; heat treatment; in situ HT-XRD; TEM; aluminides

Citation: Ott, V.; Schäfer, C.; Suarez, S.; Woll, K.; Mücklich, F.; Seifert, H.J.; Ulrich, S.; Pauly, C.; Stueber, M. Impact of Microstructure of Nanoscale Magnetron Sputtered Ru/Al Multilayers on Thermally Induced Phase Formation. *Coatings* **2023**, *13*, 149. https://doi.org/10.3390/coatings13010149

Academic Editor: Ajay Vikram Singh

Received: 8 December 2022
Revised: 23 December 2022
Accepted: 4 January 2023
Published: 11 January 2023

Copyright: © 2023 by the authors. Licensee MDPI, Basel, Switzerland. This article is an open access article distributed under the terms and conditions of the Creative Commons Attribution (CC BY) license (https://creativecommons.org/licenses/by/4.0/).

1. Introduction

Phase formation through thermal heat treatment in nanoscale metallic multilayer systems is receiving more and more attention since it often does not follow the basic laws of thermodynamics for equilibrium states and thereby offers new possibilities for microstructural design. Due to the alternating gradients, the numerous interfaces, defects (dislocations, grain boundaries, and nanovoids), etc., variations in heat and mass transports occur depending on the layer design. In addition to a change in the kinetics, this also leads to changes in the phase stability and nucleation of phases besides equilibria conditions [1–4]. Among the most important systems under consideration are Metal/Al systems for high-temperature applications, combining high oxidation resistance and strength with low density.

Different researchers have investigated such effects and developed several empirical rules for the derived phase sequences in Me/Al systems [5–7]. While these rules are relatively accurate for modulation lengths larger than 100 nm, they deviate very strictly for smaller ones. High modulation lengths can be well-described by the Pretorius' model of effective enthalpies of formation [5]. Depending on the system, phases occur stepwise,

starting with the first compound phase on the side of the element where the lowest eutectic point is located, up to the phase associated with the total stoichiometry. Systems based on nanodesign, with modulation lengths of several nanometers, are increasingly deviating from this model. Additional effects, such as nucleation barriers [6], and the influence of the interfacial volume and intermixing have to be taken into account, affecting the phase formation by the suppression of certain phases or the formation of metastable phases. One of the best-studied systems in this regard is the binary Ni/Al system, mainly known for its use in the aerospace industry. Here, of particular importance, are some of the intermetallic phases that form, which can be observed in many Me/Al combinations. Known representatives are, for example, NiAl, Ni_3Al, TiAl and FeAl. Besides good thermal conductivity [8], they offer high melting points and good oxidation resistance. Therefore, intermetallic phases in the B2 CsCl structure, such as NiAl, have long been in focus as engineering materials for high-temperature applications. A major disadvantage is their brittleness, which limits not only their processing at room temperature but also their potential applications. An interesting candidate material with improved properties is the B2 RuAl phase. It consists of two interlaced cubic primitive sublattices (CsCl structure), where each Ru atom is surrounded only by Al atoms and vice versa. It offers a high melting point of 2072 °C, increasing the temperature for possible applications, good thermal conductivity, and enhanced mechanical properties. Fleischer et al. investigated the dislocation propagation in bulk RuAl under tensile testing and demonstrated the activation of five independent slip systems. Thus, they concluded that RuAl should exhibit ductile material behavior according to the von Mises' criteria [9]. A detailed overview of the structure, properties, material behavior, and a revised phase diagram of the system was proposed by Mücklich et al. [10,11]. Furthermore, oxidation studies on co-sputtered RuAl coatings show a very good resistance up to more than 1300 °C via the formation of a stable Al_2O_3 top scale [12]. Due to the very similar coefficients of thermal expansion of the RuAl phase and the oxide scale [13], flaking of the scale can be avoided under cyclic thermal exposure [14].

The synthesis and manufacturing of bulk RuAl, however, is associated with some challenges. Due to the large differences in the melting points of the respective elements, it is difficult to produce a bulk material with a defined stoichiometry by cast metallurgy [15]. Considering, alternatively, the synthesis via a powder metallurgical route, the phase formation, microstructure, and properties in the course of heat treatment become more and more complex and depend, for example, clearly on powder particle sizes and distribution (in the range of some hundred nm up to micron sized powders) [16]. Furthermore, the powder route often suffers from porosity in the reaction product, which is detrimental for mechanical properties [17]. For this reason, such systems are extensively investigated. One way to circumvent the complex synthesis is the magnetron sputtering process. In addition to the simple synthesis of the thin film RuAl phase, the PVD process also offers the possibility of a selectively adjustable microstructure as well as the possibility of retaining the interesting properties and avoiding the brittle material behavior known for the bulk state. To investigate the phase formation in more detail, the magnetron sputtering of such multilayer thin films with a specific layer design allows the examination of microstructural and architectural effects on the phase formation during a heat treatment. There are different approaches to influence such a phase formation. Besides the classical transport effects close to thermodynamic equilibrium in large volumes with low heating rates and conversion times, the complexity extends in nanoscale systems with large chemical gradients, short transport paths, a defect-rich microstructure with many interfaces in very small volumes with high heating rates. Besides the fundamental research on the phase formation in nanoscale systems, these effects can be used specifically to create new partly metastable materials [18]. Multilayer Me/Al systems with a nanoscale design, however, are also known for their ability to initiate self-propagating reactions in case of a large negative heat of formation of the reaction product [19]. By initiating a local reaction mechanically, electrically, or thermally exceeding a critical threshold energy barrier, heat is released by the formation of intermetallic phases. Conductive heat transport leads to further propagation

of the reaction, causing the whole sample to react and the phase to form according to the overall composition [20]. Investigations of how such reactions can be controlled and what influence the design and the microstructure have on them, have been carried out mostly on Ni/Al multilayer systems. A very detailed review was published by Adams in 2015, in which he discusses in detail the different reactive thin film systems and the existing models of reactive phase formation [21]. In the case of reactive multilayer thin films in the Ru/Al-system, Pauly investigated the influence of the modulation length on the phase formation during reaction as well as the impact of adding a third element to the multilayer stack [22–24].

To investigate the phase formation in nanoscale multilayer thin films without triggering the self-propagating reaction, thermal treatments near thermal equilibrium are necessary. Zotov [25], Woll [26] and Guitar [27] showed the direct phase formation of single-phase RuAl thin films by annealing nanoscale Ru/Al multilayer thin films, with a bilayer period under 22.2 nm, near thermal equilibrium conditions without the formation of any intermediate Ru_xAl_y phases. In addition, in 2012, Woll showed in his investigations that phase formation changes as a function of bilayer thickness for this specific system. In particular, he considered the difference between small bilayers (smaller than 22.2 nm) showing the aforementioned direct phase formation toward the RuAl phase and large bilayers up to 178 nm leading to the stepwise formation of multiple Ru_xAl_y phases before the RuAl phase formed according to the overall stoichiometry [26]. Woll et al. suggested that the phase formation in Ru/Al multilayer systems should be dependent on the multilayer design and on the post-annealing.

In this work, we demonstrate that phase formation in magnetron sputtered Ru/Al multilayers can be precisely controlled and steered by the design and microstructure of the individual layers, thus suppressing the formation of individual phases. In particular, the ignition of an uncontrolled self-propagating reaction can be suppressed, and we show that the formation of a single-layer RuAl thin film in the B2 structure can be obtained via a single-step phase formation from a well-defined Ru/Al multilayer precursor by post annealing in near-equilibrium conditions. This dependence, as well as the exact description of the phase formation for different layer designs, will be further investigated and linked in this paper. This should contribute to a better understanding of nucleation processes, as well as the growth and suppression of certain phases in nanoscale systems.

2. Materials and Methods

Ru/Al multilayer thin films with systematically varied bilayer periods (see Table 1) are deposited by magnetron sputtering on a Leybold Z550 coater. Two plates made of aluminum (4N purity, FHR Anlagenbau) and ruthenium (3N purity, Kurt J. Lesker) were used as target material (75 mm diameter, 5 mm (Al) and 3 mm (Ru) thickness), which were placed in the rotationally symmetrical recipient in a 180° arrangement. The targets are bonded onto a water-cooled Cu holder. Each target is connected to a DC source, which allows to vary the power applied to the sputtering targets individually. The multilayer architecture is obtained in the top-down sputtering process by sequential deposition in a stop-and go mode via a rotating substrate plate, with a vertical distance of 50 mm to the targets. By varying the dwell time under the respective target, different layer thicknesses can be realized for the respective applied powers. The ratio of the layer thicknesses, for a total atomic composition of 1:1 Al/Ru, equals 1.22 and was considered for all multilayer thin films. Polished sapphire single crystals (c-oriented, 10 × 10 × 1 mm, Korth Kristalle GmbH) are used as substrates to avoid interaction with the layer materials during subsequent heat treatment. The substrates are cleaned with acetone before being placed in the system. Before thin film deposition, the vacuum chamber is evacuated to a residual pressure below 1×10^{-6} mbar (0.1 mPa), before the inlet of the working gas Ar 6.0.

Table 1. Listing of the synthesized Ru/Al multilayer thin films with varied nanoscale architecture.

Bilayer Period (nm)	Thin Film Thickness (μm)	Number of Bilayers	Al Layer Thickness (nm)	Ru Layer Thickness (nm)
160	4	25	88	72
40	4	100	22	18
10	4	400	5.5	4.5

The deposition on the sapphire substrates is carried out at a constant argon pressure of 0.4 Pa and an applied power of 60 W at each target, resulting in a deposition rate of 24 nm/min for Ru and 37.5 nm/min for Al and a substrate temperature of ~75 °C. Prior to coating, the sputtering targets are cleaned for 3 min at a power of 250 W per target to remove any surface contamination. A shutter prevents the substrates from being coated during this process. The shutter is also used during the sequential deposition of the multilayer structure without the usage of a substrate bias (grounded).

Phase analysis and microstructure characterization was done by X-ray diffraction (XRD) measurements on a Panalytical Empyrean system in Bragg–Brentano geometry with Cu-Kα radiation (λ = 1.540598 Å, 40 kV, 40 mA). The step size of the measurement is 0.0131° with a measuring time of 150 seconds per step. A PIXCEL3D Medipix3 1 × 1 was used as a 1D line detector with 255 channels, which allows a measurement range of 3.347° to be evaluated simultaneously. The 2-Theta range covered in these measurements was 10°–90°. The irradiated length of the sample was fixed to 8 mm by the automatic divergence slit. The assessment of the X-ray diffraction raw data was performed via the Highscore software using the ICDD PDF4+ database. Information on phase composition, crystallinity, crystalline structure, orientation, and texture formation was obtained.

To specifically investigate phase formation during heat treatment, in situ HT-XRD analysis was carried out. The XRD system mentioned above was used, equipped with an Anton Paar HTK 1200N (Anton Paar GmbH) chamber. This allows a sample to be heated under various atmospheres while simultaneously performing X-ray diffraction measurements. This is made possible by a window sealed with graphite and Kapton, which is gas-tight and temperature-resistant and at the same time permeable to X-rays. The sample was placed on a specimen holder made of corundum and equipped with a temperature sensor, in the center of the chamber. The sample is heated by radiation heating via heating elements placed at the chamber walls. After the sample loading, the chamber is sealed and purged three times with Argon 6.0, before it is evacuated to a base pressure of 10^{-2} mbar (1 Pa). This procedure is to displace the residual oxygen in the chamber and remove it by evacuation. The heat treatment and XRD measurements are then carried out in vacuum. For comparison purposes, a first XRD measurement was obtained at ambient temperature before starting the heat treatment to characterize the samples in the as-deposited state. The heating rate is set to 10 K/min. When the temperature reaches 50 °C, the temperature is maintained every 50 K and a diffractogram is recorded with a measurement time of approximately 20 min after a dwelling time of 10 minutes. The maximum temperature reached is 650 °C before cooling down. This temperature is chosen to prevent the melting of the Al phase and to consider solid state effects only.

In addition to the XRD measurements, the microstructure of the multilayers in different states was characterized using a scanning electron microscope/focused ion beam instrument (FIB/SEM, FEI Helios Nanolab600) equipped with a scanning transmission electron microscopy (STEM) detector. Furthermore, electron diffraction images were acquired in the transmission electron microscope (TEM, JEOL JEM 2010F) to verify the results from the XRD measurements. For both STEM and TEM analyses, thin lamellae were extracted by an in situ lift-out technique in the FIB/SEM, which is a common preparation routine [28]. The lamellae were mounted on a TEM lift-out grid and had an approximate width of 15 μm and a height of 5 μm. STEM imaging was performed at 30 kV with the STEM-in-SEM detector in bright field (BF), dark field (DF) and high angle annular dark field

(HAADF) mode. TEM characterization was performed with an acceleration voltage of 200 kV, and an aperture diameter of 800 nm was chosen to obtain selected area electron diffraction patterns.

3. Results

In order to investigate the thermally induced phase formation in Ru/Al multilayers, to distinguish the potential impact of the multilayer architecture and to understand the mechanisms of microstructure evolution related to the variation of the bilayer period, the results of the respective analyses are described for each thin film system. Besides the in situ X-ray diffraction, the results of the TEM and SEM are presented. Due to the amount of data obtained by the in situ HT-XRD, only the relevant diffractograms as well as the 2-Theta ranges that are directly related to phase formation are shown here.

3.1. Ru/Al Multilayers with 160 nm Bilayer Architecture

The multilayers with a bilayer period of 160 nm have the highest volume to interface fraction of all samples of this study (please note that the term interface in this case refers to phase boundaries between the two-layer materials of the as-deposited multilayers) and are considered first, as they are most likely to show the least scale effects on the phase formation. The results of the XRD analyses of the as-deposited and annealed multilayer sample with 160 nm bilayer period is shown in Figure 1. Looking at the X-ray diffraction pattern in the as-deposited state (diffractogram at T = 25°), several distinct reflections can be seen. These originate from both elemental Ru and Al in different orientations. The reflexes indicate a preferential orientation in (002) for the Ru (at ~42°), while no clear statement on the growth of Al layers during layer deposition can be made (Ru: ICDD PDF, # 00-006-0663; hexagonal, space group number: 194; Al: ICDD PDF, # 00-004-0787; cubic, space group number: 225). However, further evaluation of the Al reflections is critical for this system, because on the one hand, the scattering ability of Ru is much higher so that its reflections show considerably higher intensities, and on the other hand, because of a superposition of the (111) and the (100) reflection between 38! and 39°-2-Theta as well as the (200) and (101) reflection at 44°-2-Theta of Al and Ru, respectively. The presence of the fcc Al phase is further confirmed by the presence of the diffraction reflex at a 2-Theta angle of ~65°, which can be assigned to the (220) orientation. The initial state for the subsequent heat treatment is therefore a multilayer structure of crystalline layers of polycrystalline Ru and polycrystalline Al, with a preferred orientation for Ru. The crystallite size of the two phases can be roughly estimated via the Scherrer equation, indicating that both layer materials have nanoscale crystallite sizes in the range of 20 nm with a tendency for larger values for the Al phase.

In the course of the heat treatment of the multilayer systems, the X-ray diffraction analysis does not show any new phase formation up to an annealing temperature of 300 °C (see Figure 1 diffractograms at T = 100 and 200 °C, respectively). However, the Al reflection shows decreasing intensity in this temperature range, while the intensities of the Ru reflections remain nearly constant. Furthermore, a change of shape and shift of 37° reflection is observed. These changes in the diffractograms may indicate that a partial dissolution of the Al phase is taking place, while the signal of the Ru may as well superpose the Al signals. This is discussed in more detail in the "Discussion" section. When a temperature of 300 °C is reached, first indications of reflections of the $RuAl_6$ phase can be detected via the in situ HT-XRD ($RuAl_6$: ICCD PDF, # 04-003-1970; orthorhombic, space group number: 63). Further, the reflections of Ru are still present, with moderately lower intensities than for reflections at lower temperatures. The intensities of $RuAl_6$ diffraction reflections further increase, and additional reflections attributable to the $RuAl_6$ phase appear with increasing the temperature to 400 °C. The Ru reflections are still observed. Increasing the temperature to 500 °C results in a decrease in intensities and broadening of the diffraction reflections of the $RuAl_6$ phase, while no change of the remaining Ru reflection is detected. A very broad signal of low intensity is observed around a 2 Theta angle of 29°. This reflection cannot

be attributed to a defined phase, while it may indicate the early nucleation of the RuAl phase since the (100) orientation of the RuAl phase is in the range of the broad reflection (RuAl: ICDD PDF, # 04-004-1989; cubic, space group number: 221). At 550 °C, additional diffraction reflections of the $RuAl_2$ phase appear (not shown in Figure 1). Reaching the final temperature of 650 °C, their widths decrease, and their intensities increase, with the highest intensity for the (004) orientation. Further, diffraction reflections of the RuAl phase are observed, while the $RuAl_6$ phase can no longer be detected ($RuAl_2$: ICDD PDF, #04-003-1936; orthorhombic, space group number: 70). Elemental Ru is still present in the thin films at this annealing state, which can also be seen in the X-ray diffraction at a 2 Theta angle of ~44°. The intensity of the Ru reflections decreases with the formation of the first intermetallic phases, which are still Al-rich, and is further enhanced by the formation of Ru-richer phases. It can be stated that when the temperature of 650 °C is reached, no complete phase transformation of the elemental multilayer to the RuAl intermetallic phase can be achieved. In accordance with the overall stoichiometry, a multiphase microstructure is present in the annealed films, consisting of three phases: $RuAl_2$, RuAl and Ru.

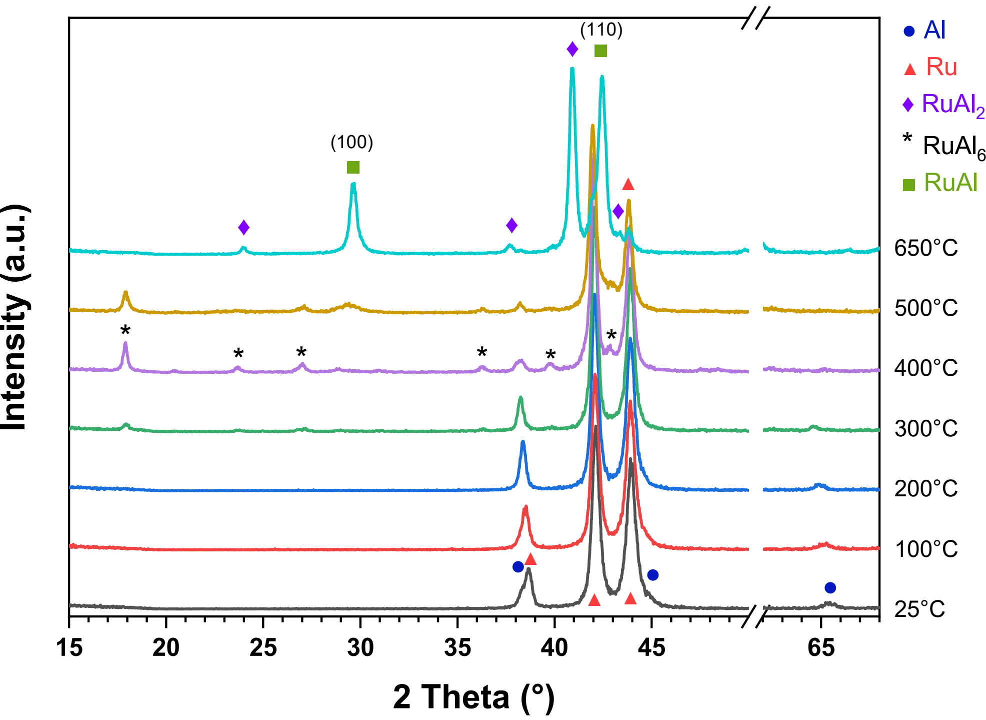

Figure 1. In situ HT-XRD analysis of the Ru/Al-multilayer thin film with a bilayer period of 160 nm for post-annealing temperatures of 25, 100, 200, 300, 400, 500 and 650 °C, respectively.

3.2. Ru/Al Multilayers with 40 nm Bilayer Architecture

Considering the phase formation via HT-XRD analysis of the thin films with 40 nm bilayer period (Figure 2), the changes in microstructure as well as in the phase evolution during annealing are different from those seen in for the multilayer films with a 160 nm bilayer period. In the as-deposited state, the films are still polycrystalline in both layers with an obtained preferred orientation 002) for Ru, while no statement can be made for the Al layers. The diffraction reflections are located at the same diffraction angles, with the slight broadening of all reflections showing lower peak intensities, indicating a smaller crystallite size of the layer materials along the growth directions (see diffractogram for T = 25 °C in Figure 2, and compare with diffractogram for T = 25 °C in Figure 1). No additional reflexes of other phases besides Ru and Al are present. The superposition of the Al diffraction reflection in (111) orientation and the Ru peak in (100) orientation is more pronounced here due to the broadening of the reflection width (FWHM). Furthermore, a

change in the intensities of the Ru reflections is obtained (compared to Figure 1), showing an increased intensity of the (101) reflection compared to the before-seen higher intensity of (002) reflection of the Ru phase. The crystallinity of the Al phase can again be verified by the presence of the (220) reflection at ~65° 2-Theta. Similar to the multilayers with the 160 nm bilayer period, the multilayers with the 40 nm bilayer period do not show new phase formation during annealing up to a temperature of 300 °C. The intensity of the Al reflection is decreasing in this temperature regime (from 25 °C to 300 °C), and the Al diffraction reflection is no longer present at 300 °C. At this temperature, multiple reflections of the $RuAl_6$ phase are observed. A superposition with diffraction reflections of the Ru_4Al_{13} phase cannot be excluded here but also not confirmed since the phases intersect in the diffraction angles for some orientations. In contrast, the existence of the $RuAl_6$ phase can be clearly demonstrated by additional diffraction reflections. These diffraction reflections exhibit a strongly increased intensity of the $RuAl_6$ phase in comparison with the before considered 160 nm bilayer thin films. The Ru phase is still present with nearly no decrease of the intensities of their diffraction reflections. Increasing the temperature to 400 °C leads to a decrease of the intensities of the $RuAl_6$ reflections and a broadening of the diffraction reflections of both the $RuAl_6$ and the elemental Ru phases. The diffraction reflections of the $RuAl_6$ phase decrease significantly in intensity as a consequence of the further temperature increase to 500 °C, suggesting a complete dissolution of this phase. At the same temperature, the first significant diffraction reflections of the RuAl phase can be detected. The Ru phase can still be indicated by the diffraction reflection at a 2-Theta angle of 42°. At the highest annealing temperature of 650 °C, a single phase RuAl thin film is obtained without the presence of the initial Ru phase, whereas the $RuAl_2$ phase does not appear. The intensity of the reflections of the desired RuAl phase increases rapidly above a temperature of 500 °C with decreasing FWHM, and a symmetrical reflection shape is obtained. The growth of the RuAl phase from the multilayer structure is not linked to a clear preferential orientation. No X-ray reflections of other phases can be detected for this annealing temperature, and a single-phase thin film is obtained with regard to the X-ray diffraction analysis.

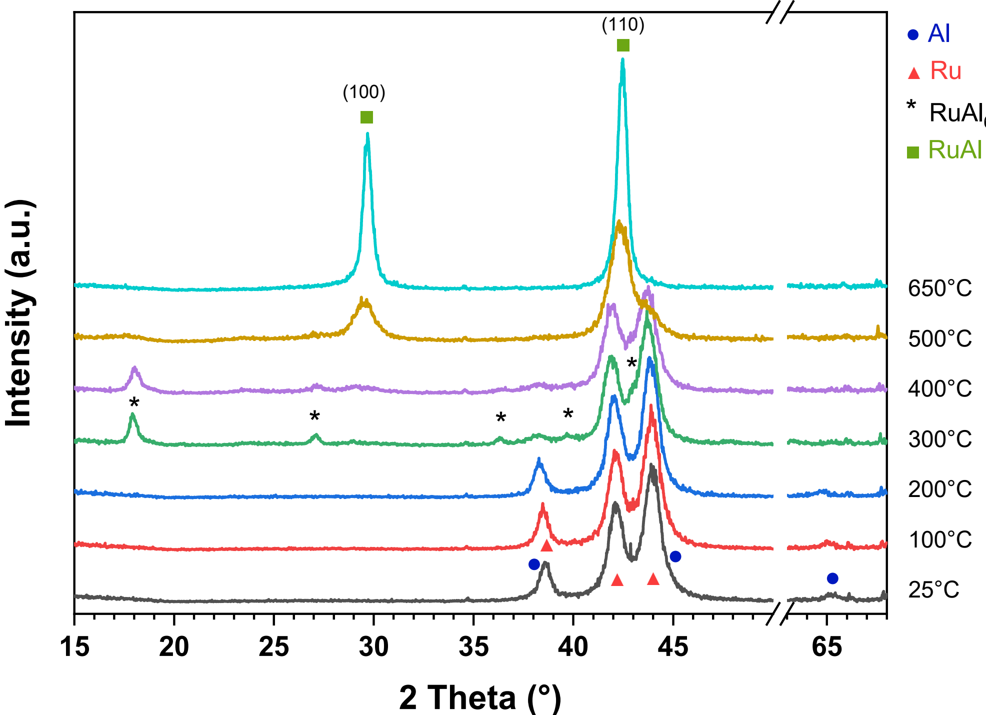

Figure 2. In situ HT-XRD analysis of the Ru/Al-multilayer thin film with a bilayer period of 40 nm for post annealing temperatures of 25, 100, 200, 300, 400, 500 and 650 °C, respectively.

Figure 3 provides more insight into the microstructure design of the Ru/Al multilayers with the 40 nm bilayer period in the as-deposited state. The microstructure of a multilayer thin film cross-sectional sample is shown: a HAADF-STEM image taken in SEM via a STEM detector is depicted in Figure 3a, TEM image is shown in Figure 3b, and the SAED patterns are shown in Figure 3c. Figure 3d shows the indexing of the diffraction rings shown in Figure 3c. The periodical multilayer structure with a bilayer period of 40 nm can clearly be seen in Figure 3a. It shows a well-defined layer structure which becomes slightly wavier with the increasing film thickness (i.e., distance of the individual layers to the sapphire substrate). In this HAADF image, the dark layers are associated to the Al phase, while the bright layers represent the Ru phase. Independent of the wavier character with an increasing number of individual layers, the overall multilayer structure remains in its periodic sequence, and there is no visible intermixing of the respective layers, which can be concluded by the sharp interfaces. Taking a closer look at the structure of the respective individual layers in the TEM image in Figure 3b, individual grains can be determined in the bright aluminum layers and in the dark Ru layers. The Al layers tend to form locally larger grains, and the thickness of the Al layers is heterogeneous, locally deviating from the originally intended layer thickness. These large Al grains seem to contribute to the disturbance of the multilayer structure, deviating from perfectly flat interfaces to more 3D-type interfaces. However, this phenomenon does not appear for the dark Ru layers, which optically show a finer microstructure with a consistent thickness. The results of the XRD analysis are also reflected in the TEM diffraction (see SAED patterns in Figure 3c). Here, only diffraction rings attributable to the Al and Ru phases can be detected. All rings are sharp and pronounced, exhibiting also individual diffraction spots. The assignment of the diffraction rings is shown in the table next to Figure 3c. Here, too, there is a partial overlapping of the diffraction rings, which is clearly visible in Figure 3c for diffraction ring 1. With the exception of the Al (220) reflection, all aluminum reflections overlap more or less strongly with ruthenium reflections, which hinders the exact evaluation since the individual rings cannot be considered separately from each other, as was already the case for the diffraction reflections of the XRD analysis. The relatively even intensity distribution in the diffraction rings indicates only little texture.

TEM investigations on 400 °C (Figure 4) and 650 °C (Figure 5) annealed multilayer thin films show the stepwise phase formation during heat treatment. Samples annealed at these temperatures were chosen to obtain information on the nucleation and growth of the intermetallic $RuAl_6$ phase as well as on the final microstructure of the emerging single-phase RuAl thin film.

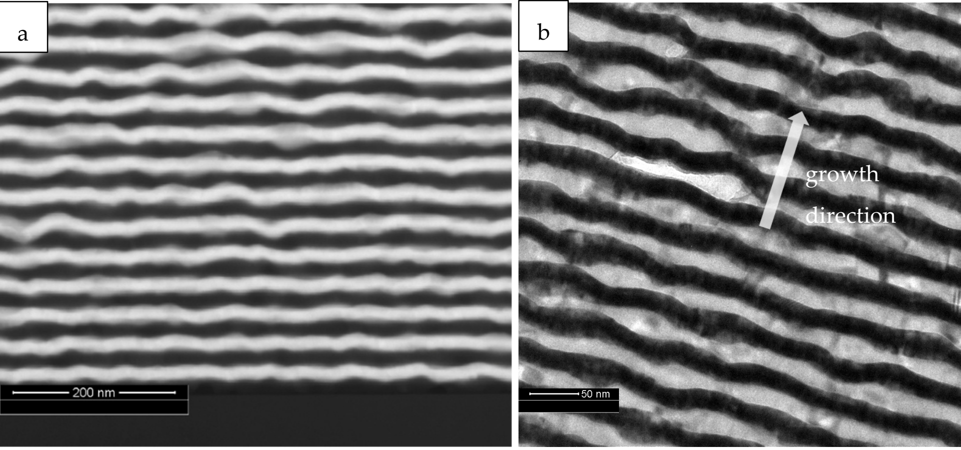

Figure 3. *Cont.*

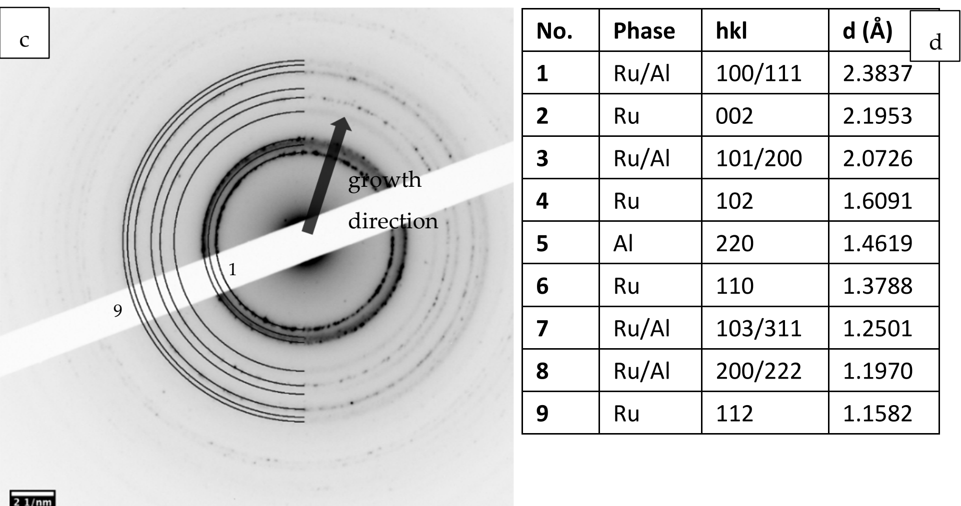

No.	Phase	hkl	d (Å)
1	Ru/Al	100/111	2.3837
2	Ru	002	2.1953
3	Ru/Al	101/200	2.0726
4	Ru	102	1.6091
5	Al	220	1.4619
6	Ru	110	1.3788
7	Ru/Al	103/311	1.2501
8	Ru/Al	200/222	1.1970
9	Ru	112	1.1582

Figure 3. Electron microscopy analysis of the multilayer Ru/Al thin film with a bilayer period of 40 nm in the as-deposited state; (**a**) STEM HAADF image of the multilayer in cross section; (**b**) TEM image of the multilayer in cross section; (**c**) SAED of the multilayer in cross section and (**d**) table with diffraction ring assignment (numbers counting from the center outwards).

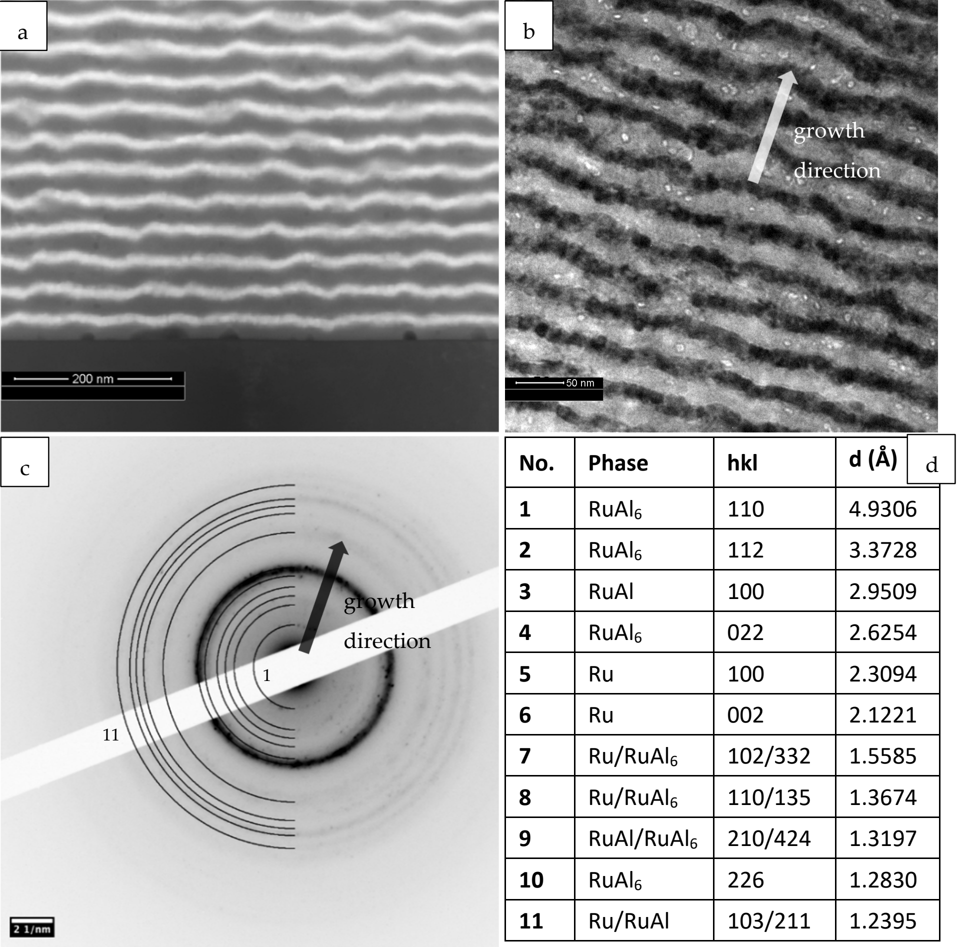

No.	Phase	hkl	d (Å)
1	$RuAl_6$	110	4.9306
2	$RuAl_6$	112	3.3728
3	RuAl	100	2.9509
4	$RuAl_6$	022	2.6254
5	Ru	100	2.3094
6	Ru	002	2.1221
7	Ru/$RuAl_6$	102/332	1.5585
8	Ru/$RuAl_6$	110/135	1.3674
9	RuAl/$RuAl_6$	210/424	1.3197
10	$RuAl_6$	226	1.2830
11	Ru/RuAl	103/211	1.2395

Figure 4. Electron microscopy analysis of the multilayer Ru/Al thin film with a bilayer period of 40 nm in annealed state at 400 °C; (**a**) STEM image of the multilayer in cross section; (**b**) TEM image of the multilayer in cross section; (**c**) SAED of the multilayer in cross section and (**d**) table with diffraction ring assignment (numbers counting from the center outwards).

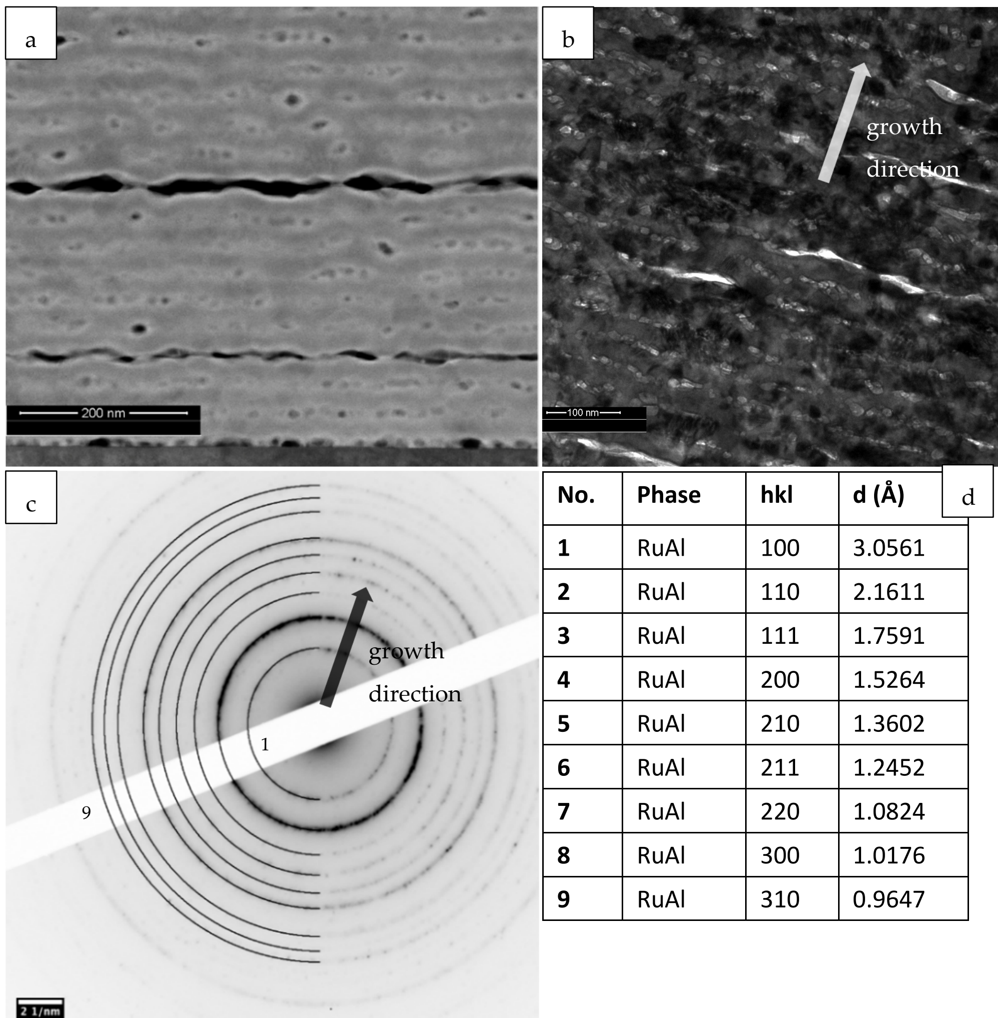

No.	Phase	hkl	d (Å)
1	RuAl	100	3.0561
2	RuAl	110	2.1611
3	RuAl	111	1.7591
4	RuAl	200	1.5264
5	RuAl	210	1.3602
6	RuAl	211	1.2452
7	RuAl	220	1.0824
8	RuAl	300	1.0176
9	RuAl	310	0.9647

Figure 5. Electron microscopy analysis of the multilayer Ru/Al thin film with a bilayer period of 40 nm in annealed state at 650 °C; (**a**) DF-STEM image of the multilayer in cross section; (**b**) TEM image of the multilayer in cross section; (**c**) SAED of the multilayer in cross section and (**d**) table with diffraction ring assignment (numbers counting from the center outwards).

In Figure 4 the results of the electron microscopy analyses are shown for a Ru/Al multilayer thin film with a bilayer period of 40 nm, annealed at a temperature of 400 °C. The HT-XRD results at 400 °C indicate a two-phase thin film composition of Ru and $RuAl_6$ phases. In the HAADF-STEM image in Figure 4a, a layered structure with two different component layers is clearly shown. This layered structure is periodical, with a local wavy appearance, similar to the structure of the as-deposited multilayer thin film. The Al layer is no longer present, and instead a distinct intermediate layer is revealed (dark grey layers), which can be assigned to the $RuAl_6$ phase by the SAED patterns shown in Figure 4b. The bright layers are assigned with the Ru phase. Furthermore, the interfaces between the layers appear well-pronounced, and the phases seem clearly separated. This is, however, a probably misleading interpretation due to the fact that with the STEM detector used, no further details can be resolved. In the TEM image in Figure 4b, the layers appear more blurred, and diffusion processes at the layer interfaces or projection artifacts can be concluded. The TEM image shows additional features represented by bright spots that are located in the center of the bright $RuAl_6$ layers, but with a more statistical distribution. This observation is discussed in more detail in section “Discussion”. The darker layers here belong to the Ru phase, while the brighter layers belong to the $RuAl_6$ phase. The SAED analysis for the annealed sample in Figure 4c shows several diffraction rings with weak

intensities near the center, as well as some with a higher distance to the center, which can be assigned to the Ru and the $RuAl_6$ phase. It must be mentioned here that the Ru_4Al_{13} phase has a strongly overlapping diffraction ring position with the $RuAl_6$ phase for some reflections. A further discussion of this is offered in the "Discussion" section. One diffraction ring with strong intensity (Nr. 6 in Figure 4c) can be observed here, which can be assigned to the Ru phase.

Samples annealed at a temperature of 650 °C show the formation of a single-phase B2 RuAl thin film microstructure in the HT-XRD (Figure 2). In Figure 5, the results of the electron microscopy analysis of a multilayer thin film with a bilayer period of 40 nm and annealed at 650 °C are shown, indicating an overall layered structure of the annealed sample, which is different from the before-discussed thin film structures. The dark field STEM image in Figure 5a shows a periodic modulation of the layer structure, with clearly visible voids or pores across the layer structure, with all layers arranged parallel to the substrate surface. This layer structure becomes apparent by different contrasts in the image, suggesting zones of different mass density (Z contrast). Further, the voids or pores are located systematically within the areas corresponding with a lower Z contrast (brighter areas). The TEM image in Figure 5b enables a more detailed insight into the microstructure. The layered structure consists of two individual layers, with an estimated modulation period of approximately 40 nm (similar to the modulation period of the as-deposited thin films). One of these layers has a thickness of approximately 30–35 nm (layers with dark contrast), while the other layer has a thickness of approximately 5–10 nm (layers with brighter contrast). In the STEM image, it can be seen that these features of lower mass thickness are located in the brighter layers which correspond to former Al layers in this case. This is further discussed in the section "Discussion". Here, we can just state that the microstructure of the 650 °C annealed thin film is heterogeneous, while very periodically arranged. The electron diffraction pattern of this sample, however, confirms only a polycrystalline single-phase B2 structure of the RuAl phase (Figure 5c), with very clearly visible diffraction rings, all of which can be assigned to the RuAl phase (Figure 5d). The layered structure could, therefore, be the result of the stepwise phase formation during the heat treatment, with the fine-grained lighter areas being the last to undergo the phase transformation to the RuAl phase.

3.3. Ru/Al Multilayers with 10 nm Bilayer Architecture

The nanoscale multilayer thin films with a bilayer period of 10 nm reflect a small-scale system with different chemical gradients, comparably small volumes of the individual phases and layers, and significantly increased internal surface areas and interface fractions (compared to the previously discussed thin films). The microstructure of the multilayer thin films in the as-deposited state is revealed by XRD analysis in Figure 6 (see diffractogram for T = 25 °C in Figure 6). Due to the small scale of the individual layers, very broad peaks are observed, which partially overlap and thus can no longer be assigned to an exact 2-Theta angle of the Al or the Ru phase. The positions of the broad diffraction reflections correspond to a superposition of the diffraction reflections of Al in (111) and Ru in (100) for the broad peak at 37° and a superposition of the diffraction reflections of Ru in (002) and (101) planes as well as the (220) planes of Al, for the reflection at ~43°. The as-deposited state can therefore be considered a nanocrystalline multilayer thin film of Ru and Al layers.

During the thermal treatment process, a different trend concerning the phase formation in the in situ HT-XRD analysis is found. The annealing of the multilayer thin film with a 10 nm bilayer period does not result in the formation of intermetallic phases up to a temperature of 400 °C. With rising temperature from 25 to 400 °C, a decrease in the intensity of the broad diffraction reflection at a 2-Theta angle of 37° is observed and is no longer detected in the diffractogram at 400 °C. Compared to the multilayers with the 160 and 40 nm bilayer period considered earlier, this effect could be attributed to the dissolution of the Al phase. The broad diffraction reflection at 43° is not affected by the annealing and retains its intensity and peak shape up to 400 °C.

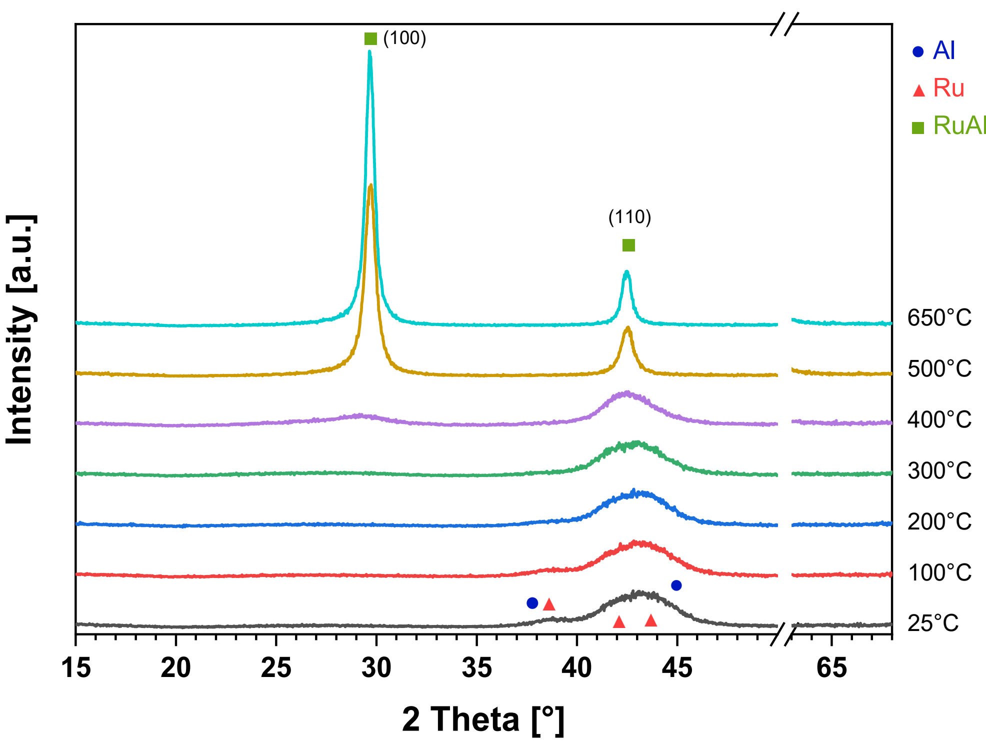

Figure 6. In situ HT-XRD analysis of the nanoscale Ru/Al-multilayer thin film with a bilayer period of 10 nm for post annealing temperatures of 25, 100, 200, 300, 400, 500 and 650 °C, respectively.

At a temperature of 400 °C, a broad reflection of very low intensity occurs around a 2-Theta angle of 29°. A diffraction reflection at 29° is characteristic of the (100) lattice plane of the RuAl phase. Additionally, the broad reflection at 43° is changed in shape and shifted slightly to lower diffraction angles, suggesting a superposition of (002) and (101) reflections of a very fine-scale Ru phase in (002) and (101) orientation and those of the emerging RuAl phase with (110) orientation. The nucleation of the RuAl phase takes place without the formation of intermediate Al-rich phases, which is a significantly different behavior than described before for the multilayer thin films with 160 and 40 nm bilayer architecture. As the temperature reaches 500 °C, two relatively sharp diffraction reflections with significantly increased intensities are observed and attributed to the B2 RuAl phase, grown in polycrystalline structure with (100) and (110) planes in diffraction condition parallel to the sample surface. No other diffraction reflections are detected. Particularly interesting here is the strong (100) reflection, indicating a preferred orientation along the film normal. At 650 °C, the intensities of all RuAl diffraction reflections increase with decreasing FWHM values, implying the grain growth of the RuAl phase with a maintained preferred orientation (100) parallel to the sample surface of the single-phase RuAl thin film.

Figure 7 shows the results of the electron microscopy analysis of a 10 nm bilayer period multilayer thin film in as-deposited state. The HAADF-STEM image in Figure 7a reveals clearly a layer structure of two separated phases, Ru (bright layers) and Al (dark layers). In contrast to the previously discussed Ru/Al multilayer thin films with a 160 and 40 nm bilayer architecture, the nanoscale multilayers show a different microstructure: their layers are deformed, resulting in a heterogeneous layered structure with a strongly pronounced wavy appearance. Since the image is taken in the center of the cross-section sample, the wavy character is possibly more pronounced. This feature is discussed in detail in the section "Discussion". The TEM image in Figure 7b, taken close to the substrate to multilayer interface, shows that the layer structure appears to have a well-separated sequential order of Al (bright layers) and Ru (dark layers), starting with more flat layers and becoming wavier with the increasing number of layers and film thickness (i.e., distance to the substrate). Thus, the TEM image confirms the observations made in the HAADF-STEM image.

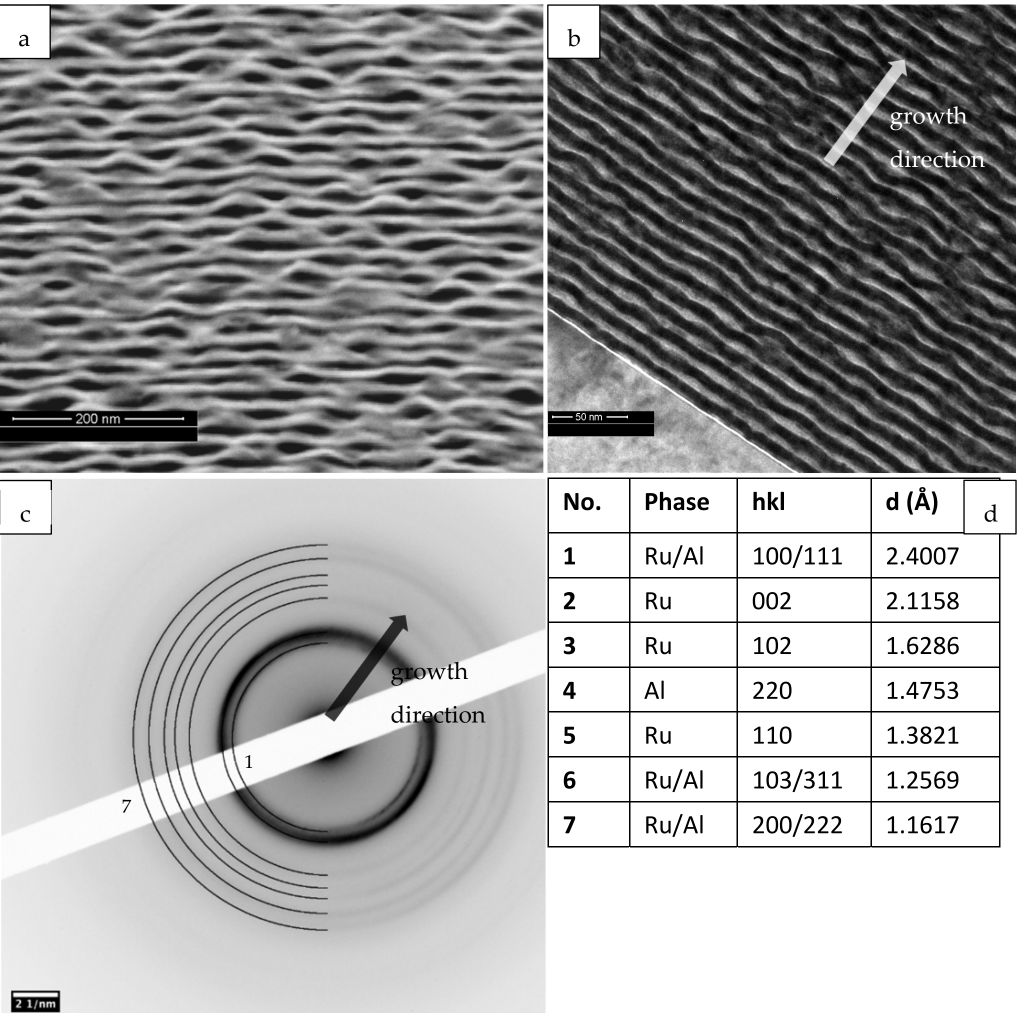

No.	Phase	hkl	d (Å)
1	Ru/Al	100/111	2.4007
2	Ru	002	2.1158
3	Ru	102	1.6286
4	Al	220	1.4753
5	Ru	110	1.3821
6	Ru/Al	103/311	1.2569
7	Ru/Al	200/222	1.1617

Figure 7. Electron microscopy analysis of the nanoscale multilayer Ru/Al thin film with a bilayer period of 10 nm in the as-deposited state: (**a**) STEM image of the multilayer in cross section; (**b**) TEM image of the multilayer in cross section; (**c**) SAED of the multilayer in cross section and (**d**) table with diffraction ring assignment (numbers counting from the center outwards).

The SAED patterns in Figure 7c verify the nanocrystallinity of the as-deposited multilayer thin film, indicated by the observation of multiple individual diffraction rings. Some of these rings are weakly pronounced and blurred. This is particularly valid for the inner two diffraction rings, which partly overlap. The rings laying further outside can be assigned to the respective phases Al and Ru, as they are indexed next to Figure 7c.

The multilayer thin film sample with a bilayer period of 10 nm annealed at 400 °C is described in Figure 8. The HAADF-STEM image in Figure 8a shows the sequential, periodical arrangement of two-layer materials, indicating a multilayer structure. A further, precise resolution of the chemical nature of these layers is not available. It can, however, be mentioned that the brighter layers should be Ru-rich ones. The TEM image in Figure 8b shows the layer structure more pronounced, and the individual layers of a Ru-rich phase (dark) and another phase (bright) can be clearly seen in a periodic configuration. No statement can be made about the formation of an intermetallic phase based on the TEM image. However, this situation is clearly resolved by the electron diffraction pattern in Figure 8c. Several diffraction rings of lower intensities and as well as two overlapping rings of higher intensities are observed. These diffraction rings can be assigned to both the Ru phase and the RuAl phase as indicated in the table next to Figure 8c; it is thus evident that the desired RuAl phase is already nucleated and grown at 400 °C, while the remaining

grains of Ru are still co-existent. The inhomogeneous intensity distribution of diffraction rings 2, 3 and 5 indicates the presence of a slight texture in Ru phase and possibly in the RuAl phase. None of the intermediate phases formed during the annealing of multilayer thin films with 160 and 40 nm bilayer architectures (i.e., $RuAl_2$ and $RuAl_6$) are formed during annealing of the multilayers with the nanoscale 10 nm bilayer architecture.

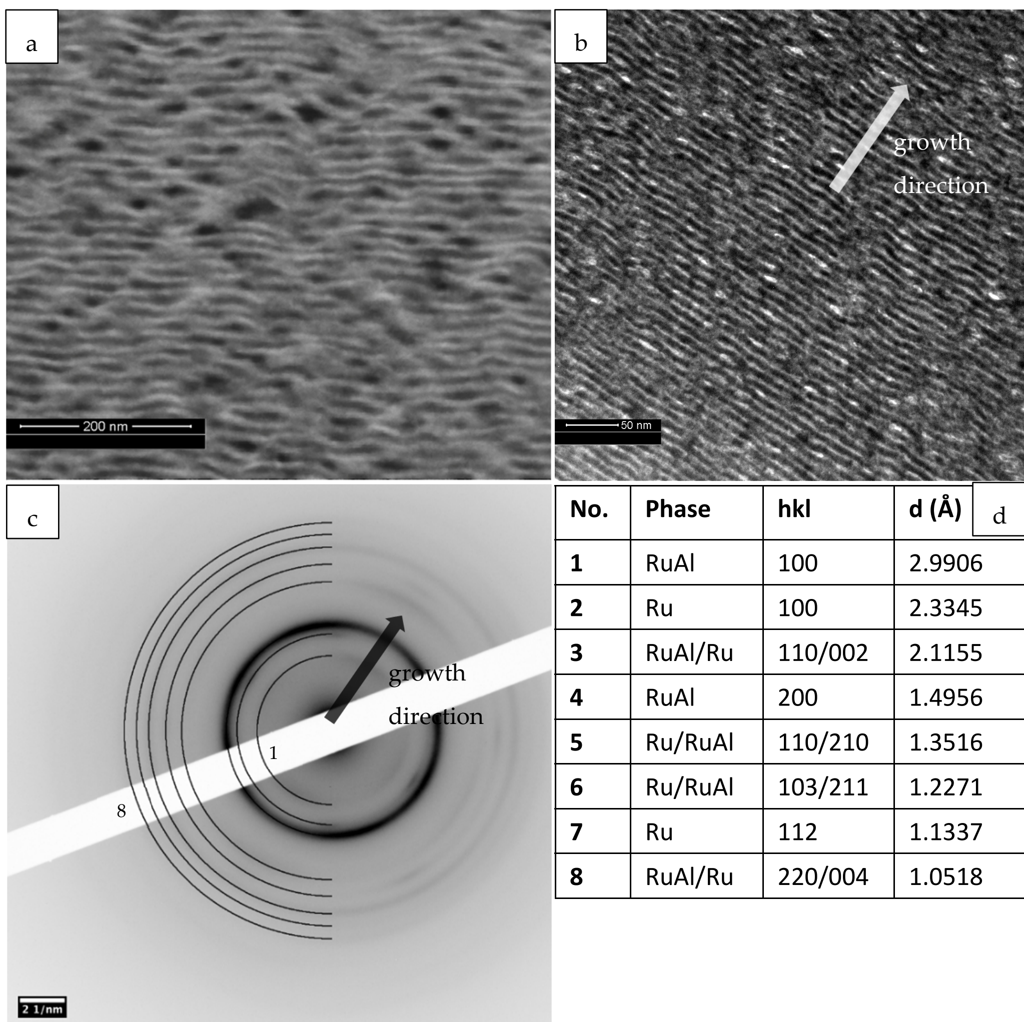

No.	Phase	hkl	d (Å)
1	RuAl	100	2.9906
2	Ru	100	2.3345
3	RuAl/Ru	110/002	2.1155
4	RuAl	200	1.4956
5	Ru/RuAl	110/210	1.3516
6	Ru/RuAl	103/211	1.2271
7	Ru	112	1.1337
8	RuAl/Ru	220/004	1.0518

Figure 8. Electron microscopy analysis of the nanoscale multilayer Ru/Al thin film with a bilayer period of 10 nm annealed at 400 °C: (**a**) STEM image of the multilayer in cross section; (**b**) TEM image of the multilayer in cross section; (**c**) SAED of the multilayer in cross section and (**d**) table with diffraction ring assignment (numbers counting from the center outwards).

The TEM analysis of the sample annealed up to temperature of 650 °C with a multilayer bilayer period of 10 nm is shown in Figure 9. The HAADF-STEM image in Figure 9a shows a uniform microstructure of the annealed thin film, without the appearance of the multilayer structure present as for the previously considered annealing state. The Z contrast differs slightly in some domains, and several darker spot-like regions are visible. The TEM image in Figure 9b shows the microstructural results for the heat treatment. Several spherical grains with different diameters up to 30 nm are obtained with a darker contrast, embedded into a lighter contrasted matrix. A rapid grain growth as well as the complete transformation to the RuAl phase must, therefore, take place between the state at an annealing temperature of 400 °C and the state at 650 °C presented here.

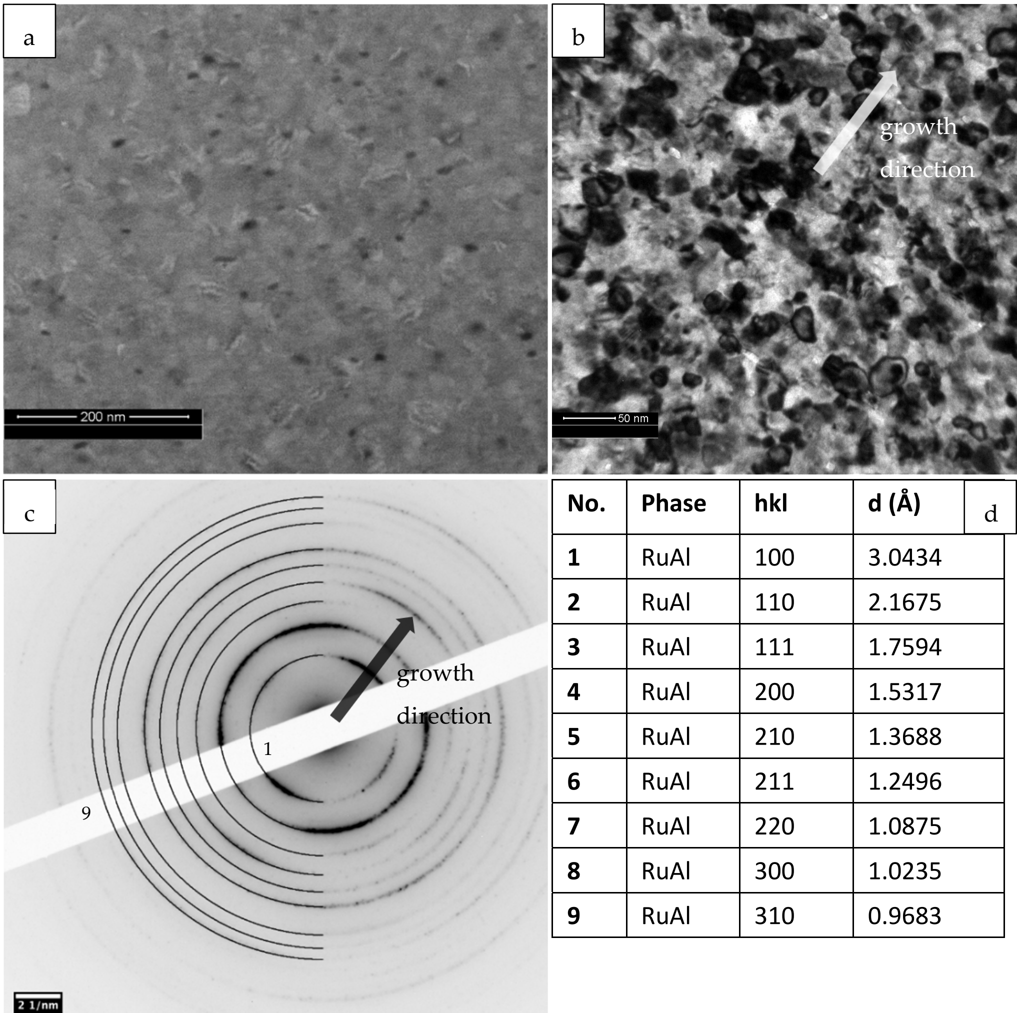

No.	Phase	hkl	d (Å)
1	RuAl	100	3.0434
2	RuAl	110	2.1675
3	RuAl	111	1.7594
4	RuAl	200	1.5317
5	RuAl	210	1.3688
6	RuAl	211	1.2496
7	RuAl	220	1.0875
8	RuAl	300	1.0235
9	RuAl	310	0.9683

Figure 9. Electron microscopy analysis of the nanoscale multilayer Ru/Al thin film with a bilayer period of 10 nm in annealed state at 650 °C: (**a**) STEM image of the multilayer in cross section; (**b**) TEM image of the multilayer in cross section; (**c**) SAED of the multilayer in cross section and (**d**) table with diffraction ring assignment (numbers counting from the center outwards).

The patterns of the SAED analysis of the annealed thin film are shown in Figure 9c. Two diffraction rings with low diffraction angles are observed with high intensities and appear segmented, indicating a texture of the obtained RuAl thin film after heat treatment. Multiple diffraction rings with lower intensities are obtained for higher diffraction angles, partly showing a segmentation. All the diffraction rings can be assigned to the RuAl phase, as it is shown by the indexing in Figure 9d.

4. Discussion

Magnetron sputtered multilayer coatings are often characterized by sharp interfaces and a nanocrystalline structure, depending on the systematics and parameters of the deposition process. This is the case for all samples analyzed in this work in the as-deposited state and is related with the low power density of ~1.36 W/cm^2 applied to the targets as well as the absence of an applied substrate bias, which results in low deposition rates and prevents strong intermixing at the layer interfaces due to the low adatomic energies of the impacting atoms. The significant differences of melting temperatures of Ru (2334 °C) and Al (660 °C) impact the growth of the individual layer materials during the sputtering process since the homologous temperature of Al (0.37) is high compared to that of Ru (0.13), which results in the growth of Al layers with larger grains, while the

Ru layers exhibit smaller grains. This corresponds well with the Thornton structure zone diagram when both layer materials grow according to a Zone T structure. In this Zone T, a fine nanoscale microstructure is observed, up to a homologous temperature of 0.3 and a coarsening microstructure for $T/T_m > 0.3$ [29]. This effect is shown by the TEM analysis of a Ru/Al multilayer thin film with 40 nm bilayer period in the as-deposited state (see Figure 3), where Al grains exceed the size of the Al layer thickness in some domains, causing an interface roughness. Thus, the periodical multilayer architecture is locally disturbed or deformed. However, a disruption of the multilayer stacking is not observed, and no direct contact between two adjacent A layers in the stacking sequence ABAB appears. Further, each nanoscale Ru layer covers the Al layer beneath completely and grows on it with homogeneous layer thickness. The interface roughness based on this effect seems even more pronounced in the Ru/Al multilayer films with a 10 nm bilayer period (see Figure 7a). In addition, further aspects of the general growth mode of the particular layer materials should also be considered. The growth of sputtered Al layers on other metal layers (as it is the case for the growth of Al on Ru) should appear according to the Stransky and Krastanov-model, with an island-type growth of the Al [30]. This should, however, be verified in future studies on the nucleation of Al layers on Ru layers and cannot be derived from the TEM analyses performed in this study. Based on the results of the TEM analysis of the as-deposited multilayer thin film with the 40 and 10 nm bilayer period shown in Figures 3 and 7, it is, however, obvious that the first deposited Al layer on the sapphire substrate is very flat, homogeneous and does not show any deformation. This indicates a dependency of the nucleation and growth mechanism of the Al layer for different sublayer materials, i.e., here, the growth of Al on single-crystalline sapphire and of Al on polycrystalline Ru. Further, the growth of aluminum layers in the face-centered cubic A1 structure on the Ru layers with a hexagonal close-packed A3 structure with preferred orientation may be associated with intrinsic stresses. These stresses would change within an individual layer material linked to the individual layer thickness. By decreasing the individual layer thickness and increasing the number of Ru/Al interfaces, however, an increase in phase boundaries is expected, leading to a change in the surface and interfacial energies, and thereby affecting the occurring stresses [31–33]. The substrate temperature does not change during the multilayer deposition, and no temperature induced growth effect has to be considered. Therefore, interface and surface energies of the respective layer materials and their influence on the nucleation and growth are the key factors for the island-like growth of the Al layers. If these growth features are related to the respective bilayer modulation lengths of the different multilayers discussed in this work, a trend toward the formation of a more heterogeneous, wavy and locally deformed interface structure is observed with the decreasing bilayer period. By decreasing the individual layer thickness (i.e., forcing the multilayer to more frequent re-nucleation of individual layers), and considering the above statements on the growth of the layers according to the structure zone model after Thornton, an increased defect concentration should be expected in the system Ru-Al. These defects may include point defects in different concentrations (i.e., vacancies) in both layer materials, grain boundaries, phase boundaries and line defects (i.e., type of dislocations, close to the phase boundaries, related to the different elastic and plastic properties of the face-centered cubic and hexagonally close-packed structured layer materials [30]).

Both X-ray diffraction and TEM diffraction of the examined multilayers show no formation of intermetallic phases in the as-deposited state for all three multilayer architectures. For multilayers with a bilayer period of 160 nm, a growth of Ru layers with a preferential orientation in (002) orientation and of the Al layers in multiple orientations is observed. This is consistent with results obtained in preliminary experiments on the magnetron sputter deposition of 4 µm thick single layer Ru thin films, where a strong texture in (002) orientation was found under the same deposition conditions, irrespective of any substrate material used. It is not consistent with the results obtained for magnetron sputtered, 4 µm thick single-layer Al thin films on different substrates (Si, sapphire, Si with oxide layer), where a preferred orientation in (111) is obtained. Therefore, the growth

of the Ru layers is energetically more favorable in (002) orientation under the selected sputtering conditions, independent of the underlying substrate material, while the strong texture of the single layers is significantly less pronounced in the case of the multilayers due to the permanent re-nucleation and competition of grains with different orientations. The growth of the Al layers is, in all studied cases, not linked to a preferred orientation. These statements apply as well to the growth of the Ru and Al layers in the multilayers with 40 nm bilayer period. In the case of the multilayer thin film with 10 nm bilayers, the X-ray diffraction is not indicative since the nanocrystallinity leads to a broadening of the diffraction reflections and they can no longer be assigned to a specific orientation of the respective layer materials. Considering the layer thickness of 5.5 nm of the Al layers as well as their lattice parameter of 0.2024 nm, it becomes clear that the layer structure consists of a maximum of approximately 25 unit-cells, resulting in a strong broadening of the peak width of the X-ray diffraction. The SAED of the TEM-analysis, however, enables a better evaluation of the phase determination and its orientations, showing multiple homogeneous intensity for both materials in different orientations. The small length scale of the individual layers should thereby prevent the preferential growth of certain orientations and lead to a nano- and polycrystalline microstructure.

Considering the thermally induced phase formation in the multilayer films with different design from the 160 to 10 nm bilayer period during vacuum annealing at 10 K/min, various effects have to be taken into account. First, the annealing at this low rate can roughly be considered to be close to thermodynamic equilibrium. Second, no self-propagating exothermic reaction is initiated in these multilayers, and all phase formations observed in this study occur completely in a solid state.

Pretorius et al. discussed the phase formation upon annealing in various, mostly physical vapor deposited Al/Me multilayer (Al/Cr, Al/Co, Al/Au, . . .) thin films [34]. They pointed out that the first phase occurring in such systems is the intermetallic phase that is closest to the eutectic point with the lowest temperature in the related binary phase diagram. This first forming phase determines the further phase formation and phase sequence during annealing. Regarding the Ru-Al system, the eutectic point is at 0.1 at.% Ru [10] adjacent to the Al single-phase area. This would imply the formation of the $RuAl_6$ phase. As shown in the section "Results", this is exactly observed and can be confirmed for Ru/Al multilayer thin films with bilayer periods of 160 nm and 40 nm. However, this model does not apply to the Ru/Al multilayer thin films with a 10 nm bilayer period in this study. Woll explicitly investigated this effect for Ru/Al multilayer thin films with bilayer thicknesses of 178 nm, dealing with magnetron sputtered thin films comparable to those of this study. He demonstrated via differential scanning calorimetry (DSC) analyses a two-step phase formation, consisting of an early nucleation step followed by a diffusion controlled growth step [26]. The nucleation process is based on the supersaturation of the Al(Ru) solid solution with approximately 15 at.% Ru before the $RuAl_6$ phase is precipitated, as it was shown by Chaudhury in vapor-deposited Al-rich Ru/Al thin films [35]. Further, the temperature required for the precipitation of $RuAl_6$ from a supersaturated Al(Ru) solid solution during the annealing of the Ru/Al multilayer thin films of the works of Zotov and Woll is determined to be ~300 °C. [25,26,35]. In addition, Pauly and Aboulfadl demonstrated the structural existence of the $RuAl_6$ phase in partially reacted Ru/Al multilayer thin films with a deviation from stoichiometry toward higher Ru contents [24,36]. This effect of an over-stoichiometric metastable $RuAl_6$ phase could prevent the nucleation of the Ru_4Al_{13} phase by an extension of the compositional range of $RuAl_6$ toward the composition of Ru_4Al_{13}. For the films with a 160 and 40 nm bilayer period shown in this work, according to the existing literature, the formation of $RuAl_6$ is also shown as the first intermetallic phase to form, and the temperature required for the formation, as it can be seen in the in-situ XRD analysis, is found to be ~300 °C. No further statements can be made concerning the nucleation of the $RuAl_6$ phase since the chosen temperature for the annealing (400 and 650 °C) of the samples for the TEM analysis is above the nucleation temperature of the $RuAl_6$ phase. However, studies by Pauly showed a clear influence of the grain

boundaries on the phase formation that occurs along the interfaces [24]. At 400 °C, the TEM analysis (see Figure 4) reveals a fully dissolved Al layer and a dense layer of $RuAl_6$ is formed instead. This supports the general theory of stepwise, temperature-dependent phase formation. Here, a detailed TEM analysis with HR-TEM for structural clarification and EELS for the elementary resolution across phase boundaries of the samples studied in this work would provide further insight into the kinetics of nucleation and the further phase formation. Additionally, a proper heat treatment with isothermal analyses below and above the threshold temperature for the formation of the specific intermetallic phases would be an interesting approach to further investigate the necessary temperatures for phase nucleation and growth. The occurrence of pores along the original Al layers in the annealed state at 400 °C can be attributed to the asymmetric material, respectively, of the vacancy transport [37]. The presence of the Ru_4Al_{13} phase, as shown by Woll, cannot be explicitly demonstrated in this work. The complexity of the phase determination here is mainly caused by the broadening of both the XRD reflections and the diffraction rings in the SAED due to the nanocrystallinity. Accordingly, only the $RuAl_6$ phase can be unambiguously detected since all diffraction reflections are present here in the diffractograms, including those that do not overlap with those of the Ru_4Al_{13} phase. The further phase formation after $RuAl_6$ should then proceed via nucleation and growth of the respective phases. The formation of the $RuAl_2$ phase as it is the case for the multilayers with a bilayer period in the range of 160 nm, is consistent with other experimental works [26]. The reduction in the modulation length of the bilayer period from 160 to 40 nm surprisingly leads to the suppression of the formation of the $RuAl_2$ phase, while in the nanoscale multilayer thin film with 10 nm bilayers, none of the intermediate intermetallics are formed, and a direct nucleation of the RuAl phase according to the overall stoichiometry takes place. This indicates that additional effects must be considered for the multilayer thin films with a bilayer period of 40 and 10 nm. The absence of certain phases during heat treatment in such nanosystems has been investigated in various works [38,39]. The influence of the interdiffusivities of the initial phases but especially of the forming phases have to principally to considered in such experiments. Since there is no evidence of the nucleation of further intermediate phases, a suppression of the phase growth can be excluded via the argumentation of different interdiffusivities of the intermetallic phases. The mechanism of the suppression of nucleation and growth of certain phases must therefore be linked to constraints such as nucleation barriers and interface effects. For diffusion processes in metals, the defect concentration as well as the chemical potential gradients take key roles. By systematically changing the bilayer period length, these factors are significantly influenced and range from comparatively steep gradients in low-defect large scale multilayer systems to rapidly changing shallow gradients in nanoscale systems with many defects. This will most likely result in a superposition of the different effects, which are both thermodynamic and kinetic in nature. The number of interfaces and their overall fraction play a decisive role both for gradient-dependent Gibbs free-energy according to Cahn and Hillard [40] and for transport processes that influence nucleation, as described by Thompson [41]. The latter concluded that phases rich in the slower diffusing species (here Al) are preferentially formed, and, moreover, phases with low interfacial energy compared to the "matrix" material are energetically more favorable for nucleation. Accordingly, the complexity and size of the crystal structure of the forming phase have a large influence on phase formation and nucleation. This changes not only the critical nucleation radius, but also the energy required to form the phase. Furthermore, Aboulfadl et al. showed that the grain boundaries play a predominant role in the nucleation in the Ru-Al system and that they also act as diffusion pathways [36]. The suppression of phase formation in the thermally heat-treated nanoscale multilayer coatings shown in this work can therefore be explained by a suppression of nucleation by kinetic barriers at the interfaces as well as by the favoring of nucleation and growth of energetically favorable phases. In addition, for nanoscale systems, due to the short diffusion paths, a very flat concentration profile is obtained. The narrow existence ranges of the intermetallic phases then result in the absence

of sufficiently large areas in the layer structure with a suitable concentration, which means that these phases cannot nucleate, and thus, phase formation is prevented. Comparing now the possible phases to form in the Ru/Al system, the RuAl phase has both the simplest crystal structure and the smallest unit cell volume among all intermediate phases, which facilitates nucleation in nano systems. This statement is supported by the early nucleation of the RuAl phase, as it is observed in the SAED of the multilayer thin film with a 10 nm bilayer period which was annealed at 400 °C (see Figure 8c). The formation of a phase in such nanosystems can thus be specifically influenced by the tool of the multilayer architecture, respectively, and the formation of certain phases can be suppressed. This opens up new ways of synthesizing alloys from multilayer thin films with specifically adjustable microstructure and furthermore enables the formation of metastable phases or supersaturated solid solutions by forcing the formation of a desired structure.

5. Conclusions

Nanoscale elemental Ru/Al multilayers with three different bilayer periods were investigated both in the as-deposited state and after vacuum heat treatment at low heating rate (10 K/min). By means of in situ HT-XRD analysis, the phase formation during thermal treatment of the samples was investigated. Based on these data, selected annealed samples were further examined by a detailed TEM analysis. It is shown that the phase sequence and the temperatures for individual phase formation correlate with the bilayer period, i.e., the nanoscale architecture of the multilayers. For multilayer coatings with a larger bilayer period (160 nm, reflecting a stacking of 170 unit cells of hcp Ru and 220 unit cells of fcc Al), a multi-stage sequential phase formation close to the thermodynamic equilibrium as described by the Ru-Al phase diagram is observed before the finally desired RuAl phase is formed according to the overall composition. In multilayers with a reduced bilayer period (40 nm, reflecting a stacking sequence of 42 unit cells of Ru and 54 unit cells of Al), some individual phases described in the phase diagram remain absent in the observed phase formation sequence upon annealing. In the case of multilayers with the smallest bilayer period investigated (10 nm, reflecting 10 unit cells of Ru and 14 unit cells of Al), the desired RuAl phase is formed directly from the elemental multilayer thin film without the formation of intermetallic intermediate phases. This suggests a dependence of mass and thermal transport on the design of nanoscale multilayers and its impact on thermodynamics and kinetics conditions during phase formation. The results of this work may contribute to a better understanding of phase formation in nanoscale multilayer systems. It suggests further that an appropriate design of such multilayer structures could provide an interesting approach by which more complex phases can be synthesized by a simply controllable thermal activation.

Author Contributions: Conceptualization, methodology: V.O. and M.S.; investigation, formal analysis, validation, data curation, visualization, project management: V.O., C.S., S.S., C.P. and M.S.; resources: F.M., H.J.S., S.U. and M.S.; writing—original draft preparation: V.O., C.S., K.W., S.U., C.P. and M.S.; writing—review and editing: V.O., C.S., K.W., F.M., H.J.S., S.U., C.P. and M.S.; supervision: F.M., H.J.S., S.U., C.P. and M.S.; funding acquisition: K.W., F.M., S.U., C.P. and M.S. All authors have read and agreed to the published version of the manuscript.

Funding: The authors V.O. and C.S. are funded by the Deutsche Forschungsgemeinschaft (DFG, German Research Foundation)—426339194. We acknowledge support by the KIT-Publication Fund of the Karlsruhe Institute of Technology.

Institutional Review Board Statement: Not applicable.

Informed Consent Statement: Not applicable.

Data Availability Statement: All data are contained within the article. Further, the data presented in this study are available on request from the corresponding authors.

Conflicts of Interest: The authors declare no conflict of interest.

References

1. Gösele, U.; Tu, K.N. Growth kinetics of planar binary diffusion couples: "Thin-film case" versus "bulk cases". *J. Appl. Phys.* **1982**, *53*, 3252–3260. [CrossRef]
2. Greer, A.L. Atomic diffusion and phase transformations in artificially layered thin films. *Scr. Metall.* **1986**, *20*, 457–464. [CrossRef]
3. Coffey, K.R.; Barmak, K. A new model for grain boundary diffusion and nucleation in thin film reactions. *Acta Metall. Mater.* **1994**, *42*, 2905–2911. [CrossRef]
4. Laskar, A.L.; Bocquet, J.L.; Brebec, G.; Monty, C. *Diffusion in Materials*; Springer: Dordrecht, The Netherlands, 1990; ISBN 978-94-010-7383-7.
5. Pretorius, R.; Marais, T.K.; Theron, C.C. Thin film compound phase formation sequence: An effective heat of formation model. *Mater. Sci. Rep.* **1993**, *10*, 1–83. [CrossRef]
6. Hodaj, F.; Gusak, A.M. Suppression of intermediate phase nucleation in binary couples with metastable solubility. *Acta Mater.* **2004**, *52*, 4305–4315. [CrossRef]
7. Bené, R.W. First nucleation rule for solid-state nucleation in metal-metal thin-film systems. *Appl. Phys. Lett.* **1982**, *41*, 529–531. [CrossRef]
8. Anderson, S.; Lang, C. Thermal Conductivity of Ruthenium Aluminide (RuAl). *Scr. Mater.* **1998**, *38*, 493–497. [CrossRef]
9. Fleischer, R.L. Intermetallic Compounds for High-Temperature Structural Use: Unique Iridium and Ruthenium Compounds. *Platin. Met. Rev.* **1992**, *36*, 138–145.
10. Mücklich, F.; Ilić, N. RuAl and its alloys. Part I. Structure, physical properties, microstructure and processing. *Intermetallics* **2005**, *13*, 5–21. [CrossRef]
11. Mücklich, F.; Ilić, N.; Woll, K. RuAl and its alloys, Part II: Mechanical properties, environmental resistance and applications. *Intermetallics* **2008**, *16*, 593–608. [CrossRef]
12. Bellina, P.J. High Temperature Oxidation of Bulk RuAl Alloy. Ph.D. Thesis, Universität Stuttgart, Stuttgart, Germany, 2006.
13. Tryon, B.; Pollock, T.M.; Gigliotti, M.; Hemker, K. Thermal expansion behavior of ruthenium aluminides. *Scr. Mater.* **2004**, *50*, 845–848. [CrossRef]
14. Woll, K.; Chinnam, R.; Mücklich, F. Thin-Film Synthesis and Cyclic Oxidation Behavior of B2-RuAl. *MRS Proc.* **2008**, *1128*, U06–U10. [CrossRef]
15. Povarova, K.B.; Morozov, A.E.; Drozdov, A.A. Heat-Resistant RuAl-Based Alloys: Part I. Cast Alloys. *Inorg. Mater. Appl. Res.* **2020**, *11*, 277–286. [CrossRef]
16. Povarova, K.B.; Morozov, A.E.; Drozdov, A.A.; Antonova, A.V.; Bulakhtina, M.A. Heat-Resistant RuAl-Based Alloys: Part II. Powder Alloys—Preparation via Reaction Sintering. *Inorg. Mater. Appl. Res.* **2021**, *12*, 1125–1138. [CrossRef]
17. Gobran, H.; Ilić, N.; Mücklich, F. Effects of particle size and pressure on the reactive sintering of RuAl intermetallic compound. *Intermetallics* **2004**, *12*, 555–562. [CrossRef]
18. Edelstein, A.S.; Everett, R.K.; Richardson, G.Y.; Qadri, S.B.; Altman, E.I.; Foley, J.C.; Perepezko, J.H. Intermetallic phase formation during annealing of Al/Ni multilayers. *J. Appl. Phys.* **1994**, *76*, 7850–7859. [CrossRef]
19. Weihs, T.P. Self-propagating reactions in multilayer materials. In *Handbook of Thin Film Process Technology*; Glocker, D.A., Ismat Shah, S., Eds.; CRC Press: Boca Raton, FL, USA, 2018; ISBN 9781351072786.
20. Munir, Z.A.; Anselmi-Tamburini, U. Self-propagating exothermic reactions: The synthesis of high-temperature materials by combustion. *Mater. Sci. Rep.* **1989**, *3*, 279–365. [CrossRef]
21. Adams, D.P. Reactive multilayers fabricated by vapor deposition: A critical review. *Thin Solid Film.* **2015**, *576*, 98–128. [CrossRef]
22. Pauly, C. Selbstfortschreitende Reaktionen in Ru/Al/X-Multilagen. Ph.D. Thesis, Universität des Saarlandes, Saarbrücken, Germany, 2017.
23. Pauly, C.; Woll, K.; Gallino, I.; Stüber, M.; Leiste, H.; Busch, R.; Mücklich, F. Ignition in ternary Ru/Al-based reactive multilayers—Effects of chemistry and stacking sequence. *J. Appl. Phys.* **2018**, *124*, 195301. [CrossRef]
24. Pauly, C.; Woll, K.; Bax, B.; Mücklich, F. The role of transitional phase formation during ignition of reactive multilayers. *Appl. Phys. Lett.* **2015**, *107*, 113104. [CrossRef]
25. Zotov, N.; Woll, K.; Mücklich, F. Phase formation of B2-RuAl during annealing of Ru/Al multilayers. *Intermetallics* **2010**, *18*, 1507–1516. [CrossRef]
26. Woll, K. Festkörper- und Selbstfortschreitende Reaktionen in Multilagen zur RuAl-Dünnschichtsynthese. Ph.D. Thesis, Universität des Saarlandes, Saarbrücken, Germany, 2012.
27. Guitar, M.A.; Aboulfadl, H.; Pauly, C.; Leibenguth, P.; Migot, S.; Mücklich, F. Production of single-phase intermetallic films from Ru-Al multilayers. *Surf. Coat. Technol.* **2014**, *244*, 210–216. [CrossRef]
28. Giannuzzi, L.A.; Kempshall, B.W.; Schwarz, S.M.; Lomness, J.K.; Prenitzer, B.I.; Stevie, F.A. FIB Lift-Out Specimen Preparation Techniques. In *Introduction to Focused Ion Beams*; Springer: Boston, MA, USA, 2005; pp. 201–228. [CrossRef]
29. Thornton, J.A. Influence of apparatus geometry and deposition conditions on the structure and topography of thick sputtered coatings. *J. Vac. Sci. Technol.* **1974**, *11*, 666–670. [CrossRef]
30. Petrov, I.; Barna, P.B.; Hultman, L.; Greene, J.E. Microstructural evolution during film growth. *J. Vac. Sci. Technol. A Vac. Surf. Film.* **2003**, *21*, S117–S128. [CrossRef]
31. Floro, J.A.; Chason, E.; Cammarata, R.C.; Srolovitz, D.J. Physical Origins of Intrinsic Stresses in Volmer–Weber Thin Films. *MRS Bull.* **2002**, *27*, 19–25. [CrossRef]

32. Wan, L.; Yu, X.; Zhou, X.; Thompson, G. Interrelationship of in situ growth stress evolution and phase transformations in Ti/W multilayered thin films. *J. Appl. Phys.* **2016**, *119*, 245302. [CrossRef]
33. Abadias, G.; Chason, E.; Keckes, J.; Sebastiani, M.; Thompson, G.B.; Barthel, E.; Doll, G.L.; Murray, C.E.; Stoessel, C.H.; Martinu, L. Review Article: Stress in thin films and coatings: Current status, challenges, and prospects. *J. Vac. Sci. Technol. A Vac. Surf. Film.* **2018**, *36*, 20801. [CrossRef]
34. Pretorius, R.; Vredenberg, A.M.; Saris, F.W.; de Reus, R. Prediction of phase formation sequence and phase stability in binary metal-aluminum thin-film systems using the effective heat of formation rule. *J. Appl. Phys.* **1991**, *70*, 3636–3646. [CrossRef]
35. Chaudhury, Z.A.; Suryanarayana, C. Metastable phases in vapour-deposited Al-Ru alloys. *J. Mater. Sci.* **1982**, *17*, 3158–3164. [CrossRef]
36. Aboulfadl, H.; Mücklich, F. Atomic-scale characterization of diffusion kinetics in Ru/Al multilayer thin films. *Mater. Lett.* **2019**, *254*, 344–347. [CrossRef]
37. Paul, A.; Laurila, T.; Vuorinen, V.; Divinski, S.V. Reactive Phase Formation in Thin Films. In *Thermodynamics, Diffusion and the Kirkendall Effect in Solids*; Paul, A., Laurila, T., Vuorinen, V., Divinski, S.V., Eds.; Springer International Publishing: Cham, Switzerland, 2014; pp. 493–528. ISBN 978-3-319-07460-3.
38. Gusak, A.M.; Lyashenko, O.Y.; Hodaj, F. The Competition of Intermediate Phases in the Diffusion Zone. *Inorg. Mater. Appl. Res.* **2019**, *10*, 517–524. [CrossRef]
39. Singh, S.; Swain, M.; Basu, S. Kinetics of interface alloy phase formation at nanometer length scale in ultra-thin films: X-ray and polarized neutron reflectometry. *Prog. Mater. Sci.* **2018**, *96*, 1–50. [CrossRef]
40. Cahn, J.W.; Hilliard, J.E. Free Energy of a Nonuniform System. I. Interfacial Free Energy. *J. Chem. Phys.* **1958**, *28*, 258–267. [CrossRef]
41. Thompson, C.V. On the role of diffusion in phase selection during reactions at interfaces. *J. Mater. Res.* **1992**, *7*, 367–373. [CrossRef]

Disclaimer/Publisher's Note: The statements, opinions and data contained in all publications are solely those of the individual author(s) and contributor(s) and not of MDPI and/or the editor(s). MDPI and/or the editor(s) disclaim responsibility for any injury to people or property resulting from any ideas, methods, instructions or products referred to in the content.